ACADEMIA ROMÂNĂ
Revue Roumaine de Chimie
http://web.icf.ro/rrch/

Rev. Roum. Chim.,
2019, *64*(4), 317-326
Doi: 10.33224/rrch.2019.64.4.04

THEORETICAL STUDY ON REACTIONS MECHANISM OF CH_3Cl WITH ClO^- AND Cl*He*O^-: A PREDICTION OF INERT-ATOM EFFECT

Liang JUNXI,* Bai JUN, Su QIONG and Zhang HUBIN

Gansu Key Laboratory of Environmental Friendly Composites and Biomass Utilization, College of Chemical Engineering, Northwest Minzu University, Lanzhou, Gansu 730030, China

Received December 18, 2017

To understand the effects of inert atom on mechanical properties, the potential energy surfaces (PESs) for the reaction of CH_3Cl with the identified Cl*He*O^- anion, together with reaction of $CH_3Cl + ClO^-$, have been computed at the BHandHLYP/aug-cc-pVDZ level of density functional theory. As a result, three kinds of chemical reactions, bimolecular nucleophilic substitution (S_N2), C-H bond insertion, and hydrogen abstraction (HAT), likely take place along the PESs. The Cl*He*O^- reaction has firstly happened through two types of mechanisms, S_N2 path and C-H bond insertion, differing from the ClO^- reaction that only initiated by a typical S_N2 fashion. Unlike the Cl*He*O^- reaction, the S_N2 pathway in the ClO^- reaction is quite facile without barriers when presence of the excess reactants. Moreover, for the ClO^- reaction two competitive substitution steps considered, S_N2-induced substitution (secondary S_N2) and HAT path, would occur with a negligible barrier before the initial S_N2 product complex separates, while for the Cl*He*O^- reaction the minimum-energy pathway proceeds as an analogous HAT path resulted from a transformation within the C-H bond-insertion product ion-dipole complex.

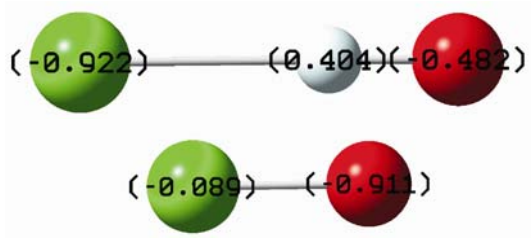

INTRODUCTION

Compound containing *Ng* (*Ng* represents rare gas element) is one of the important subjects of extensive research.[1-10] Since the *Ng* atoms have saturated electronic configuration, it is generally believed that the positively charged ions are easier to form the neutral *Ng* molecules, such as *He*H^+.[11] In contrast, there are a few examples of *Ng* containing anionic compounds, which have been attracting particular interest in research groups. Previously, Antoniotti and co-workers have, on the basis of insertion of *Ng* atom in its isoelectronic counterpart, discovered the structures of the noble gas anions F*Ng*BN^- when *Ng* on going from He to Xe.[12] As a continuation of this serial of anion's investigations, Peng *et al.* have studied the structures of the gas containing anions F*Ng*CC^- (*Ng* = He, Ar, Kr, and Xe) and predicted their stability.[13] It has been noted that the *Ng*-atom insertion type of anions are chemically bound rather than the van der Waals (vdW) complexes, although the *Ng* gas atoms are usually known to form vdW complexes.[14] Such an appropriate insertion can dramatically change electronic and chemical features of the resulting rare-atom containing anions. In general, the insertion-type *Ng* anions have a common formula, Y*Ng*X^-, where Y and X are electronegative atoms or groups. This type was also identified in 2005 by Li and co-workers, such as F*Ng*O^- (*Ng* =He, Ar, and Kr).[15] Nevertheless, in all these studies the mechanisms for the noble gas anions reactions are not explored so far, which may possess a variety of unique and unexpected properties. One example is the anion with assistance, *i.e.*, $PdCl^-$ compared to Cl^-, lowers

* Corresponding author: xbmujxliang@126.com

activation barriers and increases the exothermicity of studied reactions.[16]

Gas-phase ion-molecule studies may efficiently provide a route to gain systematic insight into the intrinsic factors that affect the reaction mechanism.[17-20] In the past decade, reactions of the conventional anion ClO^- have been well characterized experimentally and theoretically, in which the hydrogen abstraction (HAT) path acting as efficient alternative mechanism is observed besides both bimolecular nucleophilic substitution (S_N2) and base-induced bimolecular elimination (E2) pathways.[21-24] Unfortunately, to the best of our knowledge, experimental information is less available on the reactions of ClO^- with inert-atoms assistance. Theoretical investigation, an alternative way, is desirable to probe the mechanism of the types of reactions. Based on anion model of Li,[15] we report new Cl*He*O^- ion in this paper, which is derived from insertion of a *He* atom in the ClO^- anion, to perform a comparative study with ClO^- anion on the considered mechanisms provided by ClO^- reaction. In addition, studies have found that the ability of density functional methods may accurately describe negative ions,[25] particularly the hybrid DFT methods appear to be quite suitable as they provide reliable results on dipole bound anions.[26] For example, our previous researches suggest that the B3LYP exchange-correlation functional may give usefully accurate values in energy of the ClO^- S_N2 reaction.[27] Differing from our previous simulations, in this paper for the considered ClO^- + CH_3Cl reactions the typical H-atom transfer path featured in the S_N2-induced elimination reaction channel is also illustrated besides the S_N2 channel. Recent comparisons of methods show that the BHandHLYP functional not only matched well those of fairly high-level ab initio calculations,[28-30] but also gained good performance for the H-atom transfer pattern.[31] With those backgrounds, for our present studying systems two analogous reaction models, Cl*He*O^- + CH_3Cl and ClO^- + CH_3Cl, have been chosen and the corresponding investigations have been carried out using DFT-BHandHLYP level of theory. As a purpose, through this theoretical work, we hope (i) to assess how inert *He* atom interferes with the anionic electronic structure and why it causes the special change in the reaction mechanism, (ii) clarify the factors that determine transformation of reaction mechanisms, and (iii) to compare reactivity between the ClO^- reaction and the Cl*He*O^- reaction, so that yielding a better understanding of the thermodynamic and kinetic characters of Cl*He*O^- reaction.

COMPUTATIONAL METHODS

Optimization of geometries of all the studied molecules has been characterized at the DFT level of theory using the hybrid BHandHLYP functional[32-34] with the Dunning's double-zeta correlation consistent basis set with an extra diffuse function, aug-cc-pVDZ.[35,36] Harmonic vibrational frequency analysis has been performed in order to determine the nature of stationary points on the PES and to evaluate zero point energy (ZPVE) correction, which are included in the relative energies. Moreover, the intrinsic reaction coordinate (IRC) method[37] was employed to confirm the two minima connected by each transition structure when the minimum energy path (MEP) was constructed from respective saddle point geometry. Natural bond orbital (NBO)[38] analysis has been performed to get electronic population, further obtaining insights into the bonding properties. All these calculations have been done using the Gaussian 03 suite of programs.[39]

RESULTS AND DISCUSSION

With regard to the equilibrium geometries, Fig. 1 and Fig. 2 have clearly illustrated their shapes, with structural data given to some primary atoms, in which n-R, n-IM-X, n-TS-X and n-P-X are used to denote reactants, intermediates, transition states and products, respectively. Here, the number of n stands for different anion acted as reactant, namely, n = 1 for Cl*He*O^- and n = 2 for ClO^-, while the X described by the symbols S, I, and H represents the S_N2 reaction, the C-H bond insertion, and the H-atom abstraction (HAT), respectively. Moreover, to simplify the comparisons and to emphasize the trends, we have given the potential energy profiles that, starting reactants R that is set at zero as a reference, are vividly depicted in Figure 3, which are taken from the DFT-BHandHLYP level as summarized in Table 1. When comparing with the available energy information for the ClO^- reaction, as can be seen from Table 1, our BHandHLYP values are in the best agreement with the MP2 results,[23] with a largest deviation of ~13.48 kJ mol^{-1}.

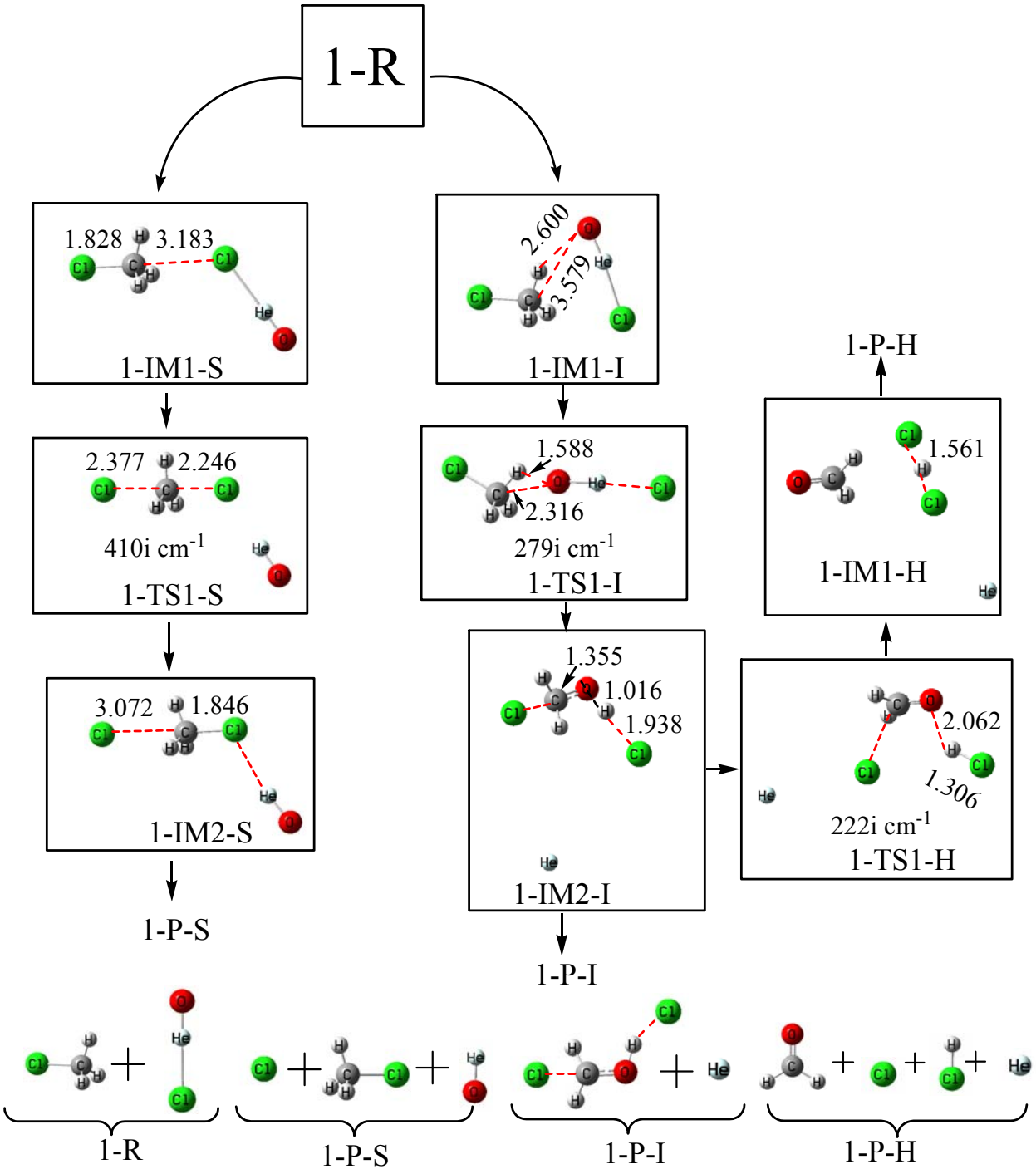

Fig. 1 – Optimized geometries of the reactions of CH_3Cl + Cl*He*O$^-$
at the BHandLYP/aug-cc-pVDZ level of theory, with bond distances Å.

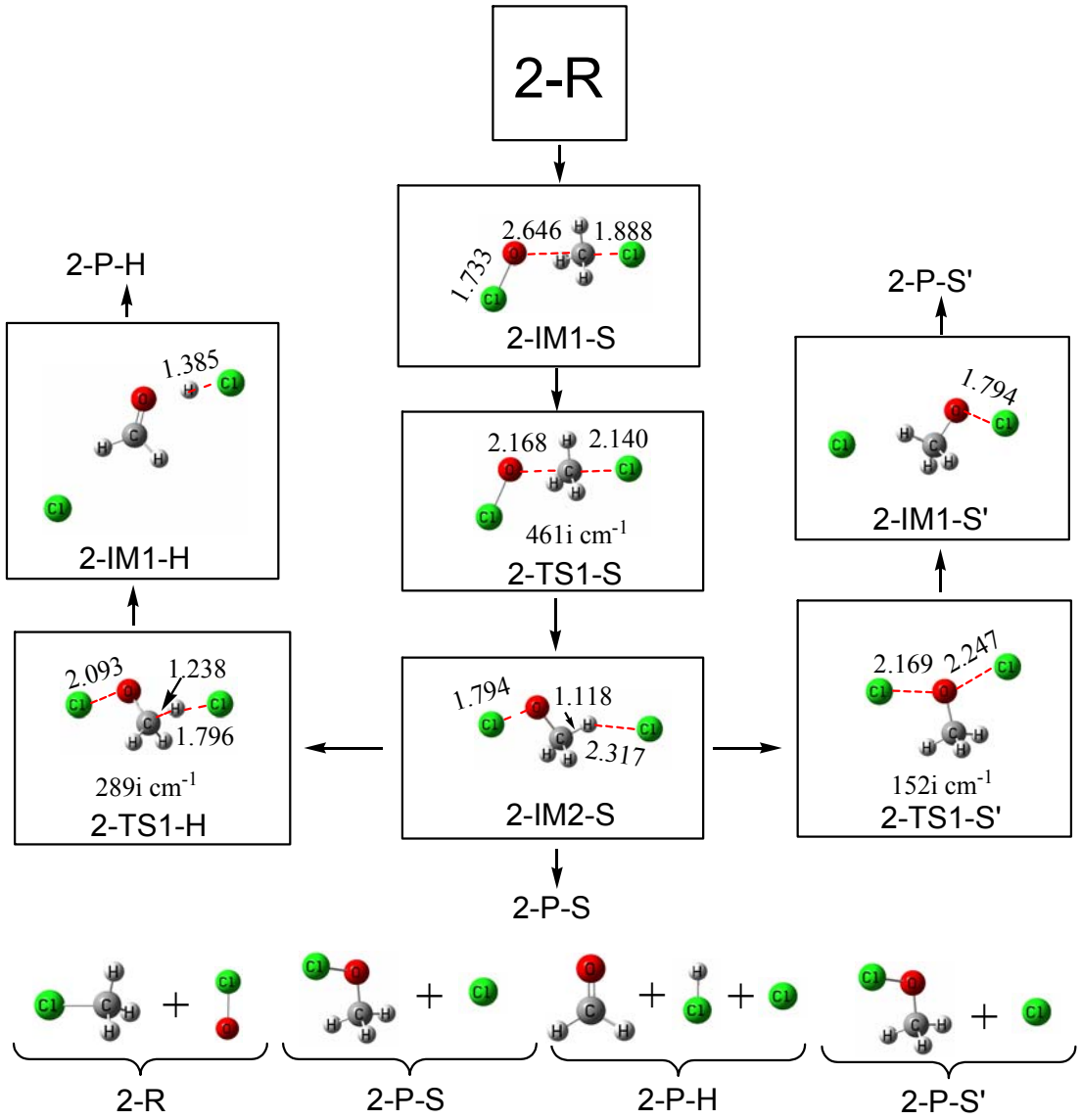

Fig. 2 – Optimized geometries of the reactions of CH_3Cl + ClO^- at the BHandLYP/aug-cc-pVDZ level of theory, with bond distances in Å.

Table 1

Electronic structure theory energies for the stationary points [Total energy E_T (a.u.), Zero-point energy E_{ZPE} (a.u.), and Relative energy E_R (kJ mol^{-1})]

ClHeO$^-$ reaction			ClO$^-$ reaction		
Species	$E_T + E_{ZPE}$	E_R	Species	$E_T + E_{ZPE}$	E_R
1-R	-1036.854598	0.00	2-R	-1035.517745	0.00
1-IM1-S	-1036.870153	-40.84	2-IM1-S	-1035.536330	-48.80 (-50.21) [a]
1-IM1-I	-1036.870985	-43.02	2-IM2-S	-1035.574167	-148.14 (-158.99) [a]
1-IM2-S	-1036.854579	0.05	2-IM1-H	-1035.664751	-385.97 (-397.48) [a]
1-IM2-I	-1037.137988	-744.04	2-IM1-S'	-1035.573876	-137.37 (-150.62) [a]
1-IM1-H	-1037.133404	-732.01	2-TS1-S	-1035.533294	-40.82 (-37.66) [a]
1-TS1-S	-1036.840624	36.69	2-TS1-H	-1035.573876	-147.37 (-133.89) [a]
1-TS1-I	-1036.851868	7.17	2-TS1-S'	-1035.556336	-101.32 (-92.05) [a]
1-TS1-H	-1037.110367	-671.52	2-P-S	-1035.555940	-100.28 (-108.78) [a]
1-P-S	-1036.830544	63.15	2-P-H	-1035.613365	-251.05 (-263.59) [a]
1-P-I	-1036.931088	-200.83	2-P-S'	-1035.555940	-100.28 (-108.78) [a]
1-P-H	-1037.115606	-685.28			

[a] Relative energies calculated at the MP2/aug-cc-pVDZ level of theory are from ref. 23.

Table 2

NBO analysis for the key stationary points [a]

	Donor		$E^{(2)}$ (kJ mol^{-1})	ΔE (a.u.)	F_{ij} (a.u.)
Cl*He*O$^-$	LP(Cl)	ceptor	47.15	0.34	0.055
		σ^*(O-H*e*)			
1-IM1-S	LP(Cl)	σ^*(O-H*e*)	39.87	0.34	0.051
1-TS1-S	LP(Cl)	σ^*(O-H*e*)	14.10	0.38	0.032
2-IM2-S	σ(C-H)	σ^*(O-Cl*)	114.01	0.31	0.087
	LP(Cl)	σ^*(O-H)	215.52	0.57	0.161
1-TS1-I	σ(C-H)	σ^*(O-*He*)	128.95	0.56	0.120
	LP(Cl)	σ^*(O-*He*)	41.84	0.14	0.035
1-IM2-I	LP(O)	σ^*(C-Cl*)	158.32	0.48	0.120
	LP(Cl)	σ^*(O-H)	183.30	0.85	0.172

[a] $E^{(2)}$ is the perurbative analysis hyperconjuagtive energy, ΔE is the energy difference between the σ and σ^* NBOs, and F_{ij} is the Fock matrix element between the NBOs *i* and *j*.

It should be noted that all kinds of reaction mechanisms of the anionic reactions are mostly dominated by the anion-reactants.[24] In this paper, our calculations have verified that the ground electronic state of the presented anions, Cl*He*O$^-$ and ClO$^-$, all were equilibrium with linear geometry ($^1\Sigma^+$) via the frequency analyses. Here, compared with the closed-shell singlet state of these reactive species, the open-shell triplet counterparts give considerably higher energies, implying less stable, which is in line with experimental observation,[40] and thus warrants to no further comments below. Our BHandHLYP/aug-cc-pVDZ Cl-O bond length of the ClO$^-$ anion (1.705 Å) is observed to be in line with the experimental data of 1.691 Å,[41] further supporting the good performance of the BHandHLYP functional for the studies system here. Analysis of the dipole moment exhibits that the Cl*He*O$^-$ (2.0484 D) possesses rather more preferential stabilization than the ClO$^-$ (2.3776 D). Such result that may originate from the role of inert-*He* atom and is very reasonable if we consider the striking hyperconjugative effect in the Cl*He*O$^-$ anion, displaying ~47.15 kJ mol^{-1} interaction, LP(Cl)$\rightarrow\sigma^*$(O-*He*), from NBO analysis collected in Table 2. In other words, the Cl*He*O$^-$ is expected to have the smaller charges separation relative to the ClO$^-$. As shown in Figure 4, for the Cl*He*O$^-$ NBO charges (a.u.) on the Cl, He, and O atoms were -0.922, 0.404, and -0.482, respectively. In contrast, the populations in the ClO$^-$ were -0.089 (Cl) and -0.911 (O), respectively. Obviously, according to nucleophilicity is determined in a straightforward manner by the electron-donor capability of the nucleophile[42], for a given substrate, one may anticipate that two different reaction fashions initiated by the Cl*He*O$^-$ take place at first, as compared with the ClO$^-$ anion. The more detailed information will be elucidated and sorted out in the following sections.

1. S_N2 pathway

As demonstrated in Fig. 1 and Fig. 2, our calculations reveal occurrence of the S_N2 reaction, *i.e.*, the ClO$^-$ reaction is considered to be achieved through its O atom close up to the C of the CH_3Cl, whereas the Cl*He*O$^-$ attack belongs to its Cl forward the CH_3Cl. As expected, a type of weakly bonded complexes, 1-IM1-S (Cl*He*O$^-$ reaction) and 2-IM1-S (ClO$^-$ reaction), were formed firstly, in excellent agreement with the nature of anion reactions,[43-47] in which geometries of the "precursor" complexes are almost unperturbed compared to the structures of the isolated reactants. Our BHandHLYP complexation energies (ΔE_{comp}), defined by the relative energy of the "precursor" complex on a particular reaction pathway in regard to the total energy of isolated one, for the two complexes are identically negative, -40.84 kJ mol^{-1} (1-IM1-S) and -48.80 kJ mol^{-1} (2-IM1-S), suggesting that formation of the complexes is quite easy with no energy requirement. By comparing the ΔE_{comp} values, it is observed that less stabilization is for 1-IM1-S associated with existence of *He* atom. NBO analysis shows (see Table 2) that for Cl*He*O segment in the 1-IM1-S structure a ~39.87 kJ mol^{-1} contribution of the interaction LP(Cl)$\rightarrow\sigma^*$(O-*He*) appears, which may results in the geometry of 1-IM1-S incompact and more relaxation, supporting less stabilization. Subsequently, further rearrangement of the intermediates 1-IM1-S and 2-IM1-S via corre-

sponding transition states described by 1-TS1-S (410i cm^{-1}) and 2-TS1-S (461i cm^{-1}) leads to the formation of the new intermediates 1-IM2-S and 2-IM2-S, accompanying breaking of the C-Cl bond of CH_3Cl molecule, especially showing *He*O moiety far away from the Cl*He*O$^-$ in the Cl*He*O$^-$ reaction. Due to existence of the inert *He* atom there is a dramatic effect on the internuclear distances of the saddle point TS. As can be obtained in Fig. 1, for Cl*He*O$^-$ reaction the breaking C-Cl* bond in the 1-TS1-S is stretched by 31% relative to its values of methane (1.809 Å), whereas the corresponding case for ClO$^-$ reaction (2-TS1-S) is 18% longer as calculated from Fig. 2. Those derive from contribution of LP(Cl)$\rightarrow\sigma^*$(O-*He*) in the 1-TS1-S structure, favoring the C-Cl* bond stretching. Here, *Cl represents the activated chlorine derived from CH_3Cl. Taken together these features indicate that the transition structure 2-TS1-S take on more reactant-like character and the barrier is encountered earlier than the 1-TS1-S. Seemingly, the reaction with Cl*He*O$^-$ exhibits a larger α-effect than that with ClO$^-$ because of later 1-TS1-S. Actually, the size of the α-effect is always smaller for the reactions with Cl*He*O$^-$ than with ClO$^-$, in which charge of the *He* atom acted as the α-atom is positive (see Fig. 4). In addition, there may be extra stability of the products with α-nucleophiles.[48] This phenomenon can be rationalized by the Hammond postulate[49] which associates an earlier transition state with a smaller barrier and a more exothermic reaction. As demonstrated below (see Fig. 3), after overcoming a barrier of only 0.02 kJ mol^{-1} the reaction of ClO$^-$ + $CH_3Cl \rightarrow ClH_3COCl^-$ (2-IM2-S) proceeds by 148.12 kJ mol^{-1} exothermicity, implying favor of the S_N2 reaction. In contrast, the reaction of Cl*He*O$^-$ + $CH_3Cl \rightarrow ClH_3CCl\cdots HeO^-$ (1-IM2-S) has indicated to undergo about 63.15 kJ mol^{-1} endothermic and its rate determining (1-IM1-S$\rightarrow$1-TS1-S) is required to overcome 77.53 kJ mol^{-1} barrier energy. Those are further borne out by our IRC calculations, as shown in Fig. 5, in the exit channel on the PES the reaction with the 2-TS1-S is very steep while the reaction with the 1-TS1-S become relatively flat. Obviously, the S_N2 reaction of Cl*He*O$^-$ is less preferred and thus the release of *Cl will occur in a difficult way. It should be noted that for the ClO$^-$ reaction before the 2-IM2-S separates two competitive steps would proceed via corresponding transition states, 2-TS1-H and 2-TS1-S', respectively. As is displayed in Fig. 2, the former named by HAT (a S_N2-induced elimination in essence) follows the abstraction of H atom by the *Cl$^-$, giving rise to the H*Cl, CH_2O, and Cl$^-$ products, which is similar to characters of alkyl nitrites reactions reported previously.[50] Alternatively, the latter named by S_N2-induced substitution is expected to undergo the displacing of the Cl of the CH_3OCl via attack of the previous leaving *Cl$^-$. Those seem to be inconsistent with Yu's theoretical results,[51] suggesting the anionic product of Cl$^-$ arises only from the S_N2-induced elimination reaction channel. In fact, localized bases favored elimination while delocalized nucleophiles favored substitution.[52] As a result, Cl$^-$ goes mainly along the HAT reaction, which is definitely confirmed by our BhandHLYP calculations. As shown in Fig. 3, relative energies of 2-TS1-H is significantly smaller than that of 2-TS1-S'. This well supports the Villano *et al.*'s investigative results, [21] proposing the occurrence of S_N2-induced elimination is favored on the energy. Our NBO analysis shows (see Table 2) that for the 2-IM2-S structure the notable hyperconjugative interaction between the σ C-H occupied orbital and the σ^*(O-Cl*) antibonding orbital, σ(C-H)$\rightarrow\sigma^*$(O-Cl*), stabilizes the staggered conformation,[53] which can be interpreted as a consequence of S_N2-induced substitution. At the same time, the other large contribution of the interactions, LP(Cl)$\rightarrow\sigma^*$(O-H), may lead to the ease of hydrogen migration, proving the occurrence of HAT pathway.

2. Insertion pathway

Our investigations have predicted that the bond insertion mechanism prefers to the reaction of Cl*He*O$^-$ than the reaction of ClO$^-$. As visualized in Fig. 3, similar to S_N2 reaction fashion mentioned above, activation of the CH_3Cl molecule driven by anion Cl*He*O$^-$ spontaneously starts to give the formation of a dipole-dipole well located by the 1-IM1-I. Subsequently, via transition state 1-TS1-I a most stable intermediate, 1-IM2-I, in this channel is formed, in which *He* atom is far away from the [Cl$\cdots$CH$_2$OH$\cdots$Cl]$^-$ group. Presuming experimental detection of the 1-IM2-I formed during the reaction is very likely because of energies of ~744.04 kJ mol^{-1} lower than the isolated reactants. Normal-mode analysis confirms that the 1-TS1-I has one and only one imaginary frequency (279i cm^{-1}), which corresponds to insertion of Cl*He*O$^-$ anion into the C-H bond of the CH_3Cl molecule. The BHandHLYP/aug-cc-pVDZ calculations predicted exothermicity of 200.83 kJ mol^{-1} for the overall insertion reaction, i.e., the 1-TS1-I should be reactant-like and the reaction channel will proceed via an "early" transition state. In fact, the typical reactant-like character for the 1-TS1-I

can also be better projected by looking at Fig. 5, which reports the Cl*He*O$^-$ reaction proceeds via 1-TS1-I with a very steep in the exit channel. Following the acceptor ability of the σ^*(O-*He*) orbital (Table 2), in 1-TS1-I the NBO second-order perturbation energy, $E^{(2)}$, for σ(C-H)$\rightarrow\sigma^*$(O-*He*) is quite sensitive, proposing ~87.11 kJ mol^{-1} higher with respect to LP(Cl)$\rightarrow\sigma^*$(O-*He*) case, to thus yield the severe activation of CH_3Cl. In this regard, the present hyperconjugative effect contributes to an "early" 1-TS1-I. Next, there are two branching processes from 1-IM2-I: one is direct elimination of the *He* atom with no intrinsic barrier to yield the end products $[Cl^{\cdots}CH_2OH^{\cdots}Cl]^-$ + *He*, and another is formation of the products CH_2O + $[Cl^{\cdots}HCl]^-$ + *He* via transition state 1-TS1-H (222i cm^{-1}), involving both H-abstraction and isomerization. Comparing the energy variation on the PES, the latter is asserted to be more favorable than the former because the 1-TS1-H lies below insertion product 1-P-I by 470.69 kJ mol^{-1} energies calculated at the BHandHLYP/aug-cc-pVDZ level of theory. Although energies of the insertion-product are quite high, it can produce readily since the 1-P-I is considerably lower in energies than the reactants asymptote, by 200.83 kJ mol^{-1}.

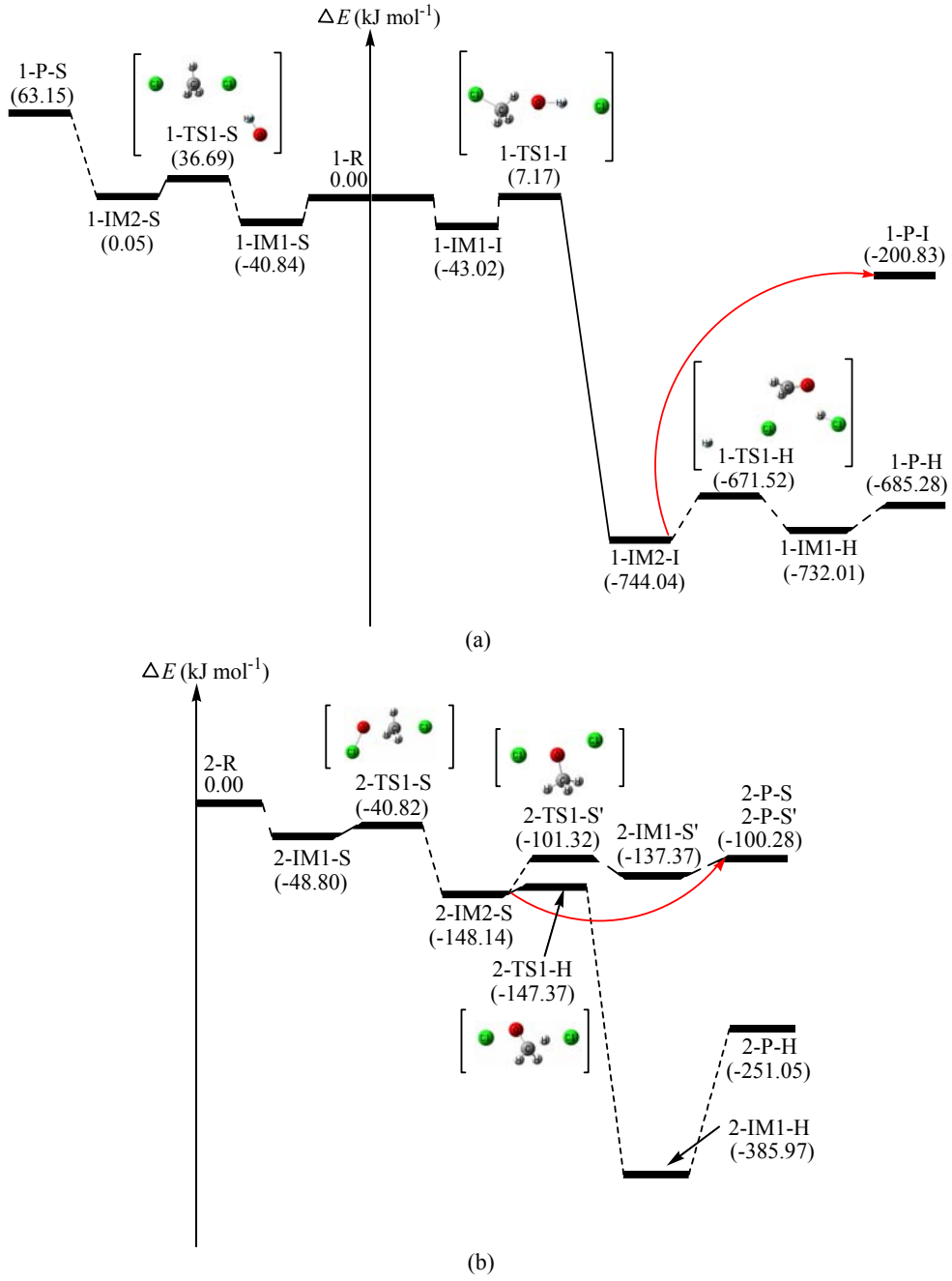

Fig. 3 – Energy profiles for (a) the Cl*He*O$^-$ reactions and (b) the ClO$^-$ reactions.

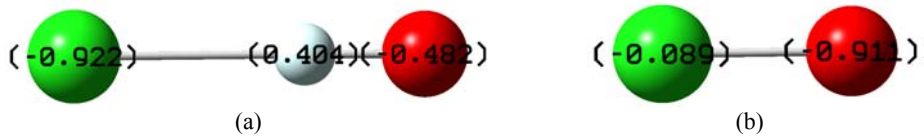

(a) (b)

Fig. 4 – NBO charges (a.u.) assigned to the reactants (a) Cl*He*O$^-$ and (b) ClO$^-$.

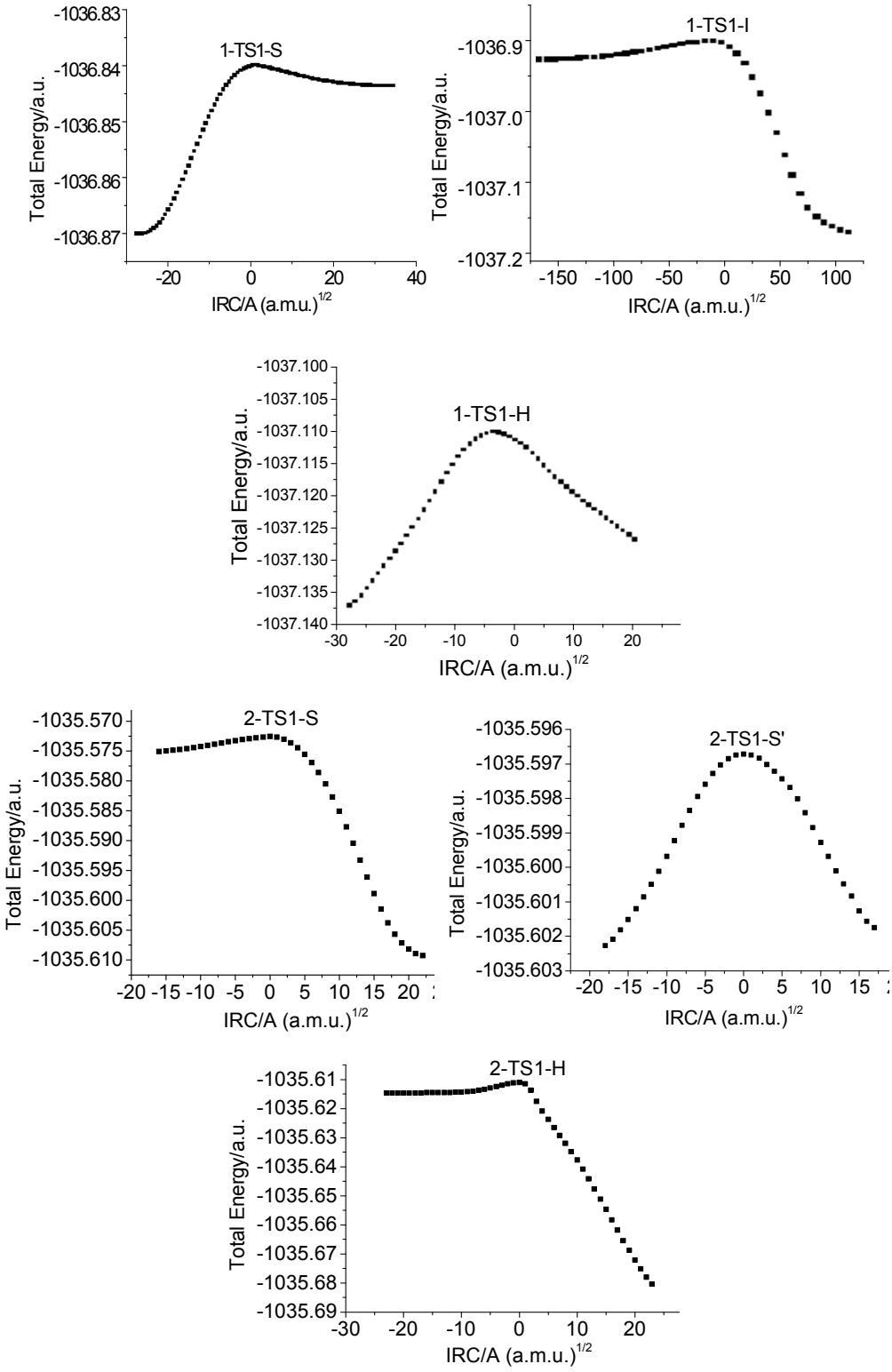

Fig. 5 – Potential energy profiles for the associated pathways along the coordinates.

3. HAT pathway

According to the thermodynamics of the system that may make the lifetime of the complexes relatively long, allowing for additional chemistry to occur,[54] for ClO^- reaction starting from 2-IM2-S the H-abstraction can happen, namely, the path occurs by the migrating of hydrogen-atom from the $Cl^{\cdots}OCH_3$ group to $^*Cl^-$ via the transition state 2-TS1-H, following the Cl-O bond breaking, to form stable intermediate 2-IM1-H characterized by ~385.97 kJ mol^{-1} low the zero-energy level, which invariably facilitates the generation of the final products (CH_2O + H^*Cl + Cl^-). Likewise, the corresponding finding was also proven in the Cl*He*O^- reaction, as a result of HAT pathway as mentioned in the section **3.2**, the reaction beginning from intermediate 1-IM2-I was expected to proceed via transition state 1-TS1-H (H-abstraction and isomerization in a concerted step) to yield the end product 1-P-H (CH_2O + HCl + Cl^- + *He*), which is energetically most favored. NBO analysis found for the 1-IM2-I structures, as listed in Table 2, displays two main contribution of the interactions (the donor of the nonbonding electrons), $LP(O) \rightarrow \sigma^*(C\text{-}Cl^*)$ and $LP(Cl) \rightarrow \sigma^*(O\text{-}H)$, respectively. The former yields a decreasing stabilization of the staggered conformation, similar to the results proposed by Bundhun *et al.*,[55] while the latter leads to the ease of HAT and so to support H-abstraction pathway. Although the potential barrier from 1-IM2-I to 1-TS1-H, ~62.52 kJ mol^{-1}, is quite high, it can proceed readily since the 1-TS1-H is predicted to be 671.52 kJ mol^{-1} lower in energy than the separated reactants and its heat of reaction is approximately 685.28 kJ mol^{-1}. In contrast, occurrence of HAT path of the ClO^- reaction requires a 0.75 kJ mol^{-1} barrier via 2-TS1-H with an energy release of 251.05 kJ mol^{-1}. Apparently, the HAT in the ClO^- reaction takes place more readily. Meanwhile, another pinpointed feature in this reaction is to be that the appearance of the predicted product-complex 2-IM1-H may be dominant at high temperature and low pressure because of its 385.97 kJ mol^{-1} lower energies with respect of zero-energy reference.

4. The most favored channel

Possible pathways obtained for the most favored channels of the Cl*He*O^- and ClO^- reactions are of different, however, as also depicted in Fig. 3, somewhat similar step identified by HAT occurs. Calculated energy profiles show that Cl*He*O^- reaction starts via the C-H bond insertion whereas it becomes S_N2 pathway for ClO^- reaction. Nevertheless, as the above-mentioned in this paper, pathway of the bond insertion (1-TS1-I) through the Cl*He*O^- is characterized by higher energy barriers than that of S_N2 (2-TS1-S) in the ClO^- reaction. Such higher barrier height of 1-TS1-I can stem from more strength of C-H bond activation compared to C-Cl bond case. Furthermore, as shown in Fig. 1 and Fig. 2, the 2-TS1-S could possess higher stability because of the presence of a linear $O^{\cdots}C^{\cdots}Cl$ structure, whereas the 1-TS1-I is less stable owing to formation of less stable strained three-membered ring geometry. However, a noteworthy fact here is that the complex 1-IM2-I is located substantial below the zero-energy level compared to the separated reactants (~744.04 kJ mol^{-1}; see Fig. 3), specifically, ~595.92 kJ mol^{-1} lower in energy than the 2-IM2-S. It supports that additional chemistry emanating from can subsequently occur.

Acknowledgment. This research has been supported by the Fundamental Research Funds for the Central Universities (31920190073) and the Chemistry-Key Discipline Construction of Gansu Province.

CONCLUSION

In summary, the reaction mechanisms of ClO^- /Cl*He*O^- with CH_3Cl have been comparatively analyzed at the DFT-BHandHLYP level of theory using aug-cc-pVDZ basis set. On the basis of our simulations, comparing to ClO^- reaction case, three different reaction mechanisms, S_N2, bond insertion, and HAT, are revealed for the anionic reaction of Cl*He*O^- as a result of the insertion of helium atom, in which the occurrence of HAT mechanism is the most favored. The detailed conclusions are as following: (1) the Cl*He*O^- anion possesses rather more preferential stabilization than the ClO^- due to the striking hyperconjugative effect. (2) The ClO^- and Cl*He*O^- reactions can uniformly initiated by a typical S_N2 fashion at first, in which the latter exhibit less reactivity than the former because of the smaller size of the α-effect originated from the bonded *He* atom (3) pathway of C-H bond insertion only appears in the reaction of Cl*He*O^- + CH_3Cl because $\sigma(C\text{-}H) \rightarrow \sigma^*(O\text{-}He)$ is quite sensitive presented here, in comparison with the ClO^- + CH_3Cl reaction. (4) compared with the ClO^- reaction, the MEP for the Cl*He*O^- reaction proceeds as an analogous HAT pathway before the C-H bond-insertion product complex separates.

REFERENCES

1. M. Pettersson, J. Lundell and M. Räsänen, *J. Chem. Phys.*, **1995**, *102*, 6423-6431.
2. M. Pettersson, J. Lundell, L. Khriachtchev and M. Räsänen, *J. Chem. Phys.*, **1998**, *109*, 618-625.
3. M. Pettersson, J. Lundell, L. Khriachtchev, E. Isoniemi and M. Räsänen, *J. Am. Chem. Soc.*, **1998**, *120*, 7979-7980.
4. T. K. Ghanty, *J. Chem. Phys.*, **2005**, *123*, 074323-074329.
5. M. Pettersson, L. Khriachtchev, J. Lundell and M. Räsänen, *J. Am. Chem. Soc.*, **1999**, *121*, 11904-11905.
6. T. Jayasekharan and T. K. Ghanty, *J. Chem. Phys.*, **2008**, *129*, 184302-184309.
7. T. Jayasekharan and T. K. Ghanty, *J. Chem. Phys.*, **2012**, *136*, 164312-164319.
8. A. Ghosh, D. Manna and T. K. Ghanty, *J. Chem. Phys.*, **2013**, *138*, 194308-194315.
9. A. Sirohiwal, D. Manna, A. Ghosh, T. Jayasekharan and T. K. Ghanty, *J. Phys. Chem. A*, **2013**, *117*, 10772-10782
10. T. Arppe, L. Khriachtchev, A. Lignell, A. V. Domanskaya and M. Räsänen, *Inorg. Chem.*, **2012**, *51*, 4398-4402.
11. F. Grandinetti, *Int. J. Mass Spectrom.*, **2004**, *237*, 243-267.
12. P. Antoniotti, S. Borocci, N. Bronzolino, P. Cecchi and F. Grandinetti, *J. Phys. Chem. A*, **2007**, *111*, 10144-10151.
13. C.-Y. Peng, C.-Y. Yang, Y.-L. Sun and W.-P. Hu, *J. Chem. Phys.*, **2012**, *137*, 194303-194309.
14. D. Manna, A. Ghosh and T. K. Ghanty, *J. Phys. Chem. A*, **2013**, *117*, 14282-14292.
15. T.-H. Li, C.-H. Mou, H.-R. Chen and W.-P. Hu, *J. Am. Chem. Soc.*, **2005**, *127*, 9241-9245.
16. A. Diefenbach, G. T. de Jong and F. M. Bickelhaupt, *J. Chem. Theory Comput.*, **2005**, *1*, 286-298.
17. G. I. Mackay and D. K. Bohme, *J. Am. Chem. Soc.*, **1978**, *100*, 327-329.
18. W. N. Olmstead and J. I. Brauman, *J. Am. Chem. Soc.*, **1977**, *99*, 4219-4228.
19. J. I. Brauman and L. K. Blair, *J. Am. Chem. Soc.*, **1970**, *92*, 5986-5992.
20. J. S. Brodbelt, J. Isbell, J. M. Goodman, H. V. Secor and J. I. Seeman, *Tetrahedron Lett.*, **2001**, *42*, 6949-6952.
21. S. M. Villano, S. Kato, W. C. Lineberger and V. M. Bierbaum, *J. Am. Chem. Soc.*, **2006**, *128*, 736-737.
22. W. P. Hu and D. G. Truhlar, *J. Am. Chem. Soc.*, **1996**, *118*, 860-869.
23. S. M. Villano, N. Eyet, W. C. Lineberger and V. M. Bierbaum, *J. Am. Chem. Soc.*, **2009**, *131*, 8227-8233.
24. J.-X. Liang, Y.-B. Wang, Q. Zhang, Y. Li, Z.-Y. Geng and X.-H. Wang, *J. Mol. Model.*, **2013**, *19*, 1739-1750.
25. J. M. Galbraith and H. F. Schaefer III, *J. Chem. Phys.*, **1996**, *105*, 862-864.
26. Y. Bouteiller, C. Desfrancüois, J. P. Schermann, Z. Latajka and B. Silvi, *J. Chem. Phys.*, **1998**, *108*, 7967-7972.
27. J.-X. Liang, Q. Su, Y. Li, Q. Zhang and Z.-Y. Geng, *Can. J. Chem.*, **2014**, *92*, 868-875.
28. U. Wille and T. Dreessen, *J. Phys. Chem. A*, **2006**, *110*, 2195-2203.
29. U. Wille, J. C.-S. Tan and E. K. Mucke, *J. Org. Chem.*, **2008**, *73*, 5821-5830.
30. S. H. Kyne, C. H. Schiesser and H. Matsubara, J. Org. Chem., **2008**, *73*, 427-434.
31. J.-X. Liang, Q. Su, D.-Z. Zhao, Y.-B. Wang, G.-H. Li and Z.-Y. Geng, *Heteroatom Chem.*, **2016**, *27*, 199-209.
32. P. J. Stephens, F. J. Devlin, C. F. Chabalowski and M. J. Frisch, *J. Phys. Chem.*, **1994**, *98*, 11623-11627.
33. A. D. Becke, *J. Chem. Phys.*, **1993**, *98*, 5648-5652.
34. C. Lee, W. Yang, and R. G. Parr, *Phys. Rev. B* **1988**, *37*, 785-789.
35. R. A. Kendall, T. H. Dunning Jr and R. J. Harrison, *J. Chem. Phys.*, **1992**, *96*, 6796-6806.
36. T. H. Dunning Jr, K. A. Peterson and A. K. Wilson, *J. Chem. Phys.*, **2001**, *114*, 9244-9253.
37. K. Fukui, *Acc. Chem. Res.*, **1981**, *14*, 363-368.
38. A. E. Reed, L. A. Curtiss and F. Weinhold, *Chem. Rev.*, **1988**, *88*, 899-926.
39. M. J. Frisch, G. W. Trucks, H. B. Schlegel, G. E. Scuseria, M. A. Robb, J. R. Cheeseman, J. A. Montgomery, T. Vreven Jr, K. N. Kudin, J. C. Burant, J. M. Millam, S. S. Iyengar, J. Tomasi, V. Barone, B. Mennucci, M. Cossi, G. Scalmani, N. Rega, G. A. Petersson, H. Nakatsuji, M. Hada, M. Ehara, K. Toyota, R. Fukuda, J. Hasegawa, M. Ishida, T. Nakajima, Y. Honda, O. Kitao, H. Nakai, M. Klene, X. Li, J. E. Knox, H. P. Hratchian, J. B. Cross, V. Bakken, C. Adamo, J. Jaramillo, R. Gomperts, R. E. Stratmann, O. Yazyev, A. J. Austin, R. Cammi, C. Pomelli, J. W. Ochterski, P. Y. Ayala, K. Morokuma, G. A. Voth, P. Salvador, J. J. Dannenberg, V. G. Zakrzewski, S. Dapprich, A. D. Daniels, M. C. Strain, O. Farkas, D. K. Malick, A. D. Rabuck, K. Raghavachari, J. B. Foresman, J. V. Ortiz, Q. Cui, A. G. Baboul, S. Clifford, J. Cioslowski, B. B. Stefanov, G. Liu, A. Liashenko, P. Piskorz, I. Komaromi, R. L. Martin, D. J. Fox, T. Keith, M. A. Al-Laham, C. Y. Peng, A. Nanayakkara, M. Challacombe, P. M. W. Gill, B. Johnson, W. Chen, M. W. Wong, C. Gonzalez and J. A. Pople, Gaussian 03 (Revision E.01), Gaussian, Inc., Wallingford CT, **2004**.
40. L. C. Lee, G. P. Smith, J. T. Moseley, P. C. Cosby and J. A. Guest, *J. Chem. Phys.*, **1979**, *70*, 3237-3246.
41. B. Armando, A. S. N. Juan and S. Bernard, *J. Phys. Chem. A*, **1999**, *103*, 3078-3088.
42. A. P. Bento and F. M. Bickelhaupt, *J. Org. Chem.*, **2008**, *73*, 7290-7299.
43. D. E. Applequist and A. H. Peterson, *J. Am. Chem. Soc.*, **1961**, *83*, 862-865.
44. D. Kapeller, R. Barth, K. Mereiter and F. Hammerschmidt, *J. Am. Chem. Soc.*, **2007**, *129*, 914-923.
45. Y. Nobe, K. Arayama and H. Urabe, *J. Am. Chem. Soc.*, **2005**, *127*, 18006-18007.
46. V. M. Bierbaum, C. H. DePuy and R. H. Shapiro, *J. Am. Chem. Soc.*, **1977**, *99*, 5800-5802.
47. S. R. Kass, J. J. Filley, M. V. Doren and C. H. Depuy, *J. Am. Chem. Soc.*, **1986**, *108*, 2849-2852.
48. Y. Ren and H. Yamataka, *Chem. Eur. J.* **2007**, *13*, 677-682
49. G. S. Hammond, *J. Am. Chem. Soc.*, **1955**, *77*, 334-338.
50. A. J. Noest and N. M. M. Nibbering, *Adv. Mass Spectrom.*, **1980**, *8*, 227-237.
51. F. Yu, *J. Phys. Chem. A*, **2016**, *120*, 1813-1818
52. S. Gronert, *Acc. Chem. Res.*, **2003**, *36*, 848-857.
53. L. C. Song, Y. C. Lin, W. Wu, Q. Zhang and Y. Mo, *J. Phys. Chem. A*, **2005**, *109*, 2310-2316.
54. C. H. DePuy and V. M. Bierbaum, *J. Am. Chem. Soc.*, **1981**, *103*, 5034-5038.
55. A. Bundhun, P. Blowers, P. Ramasami and H. F. Schaefer III, *J. Phys. Chem. A*, **2010**, *114***,** 4210-4223.